Journal of
Applied Crystallography
ISSN 0021-8898

Received 23 September 1999
Accepted 28 April 2000

X-ray diffraction from perfect silicon crystals distorted by surface acoustic waves

R. Tucoulou,[a]* R. Pascal,[a] M. Brunel,[a]† O. Mathon,[b] D. V. Roshchupkin,[c] I. A. Schelokov,[c] E. Cattan[d] and D. Remiens[d]

[a]Laboratoire de Cristallographie, CNRS, BP166, 38043 Grenoble CEDEX 9, France, [b]ESRF, BP220, 38042 Grenoble CEDEX 9, France, [c]Institute of Microelectronic Technology, Russian Academy of Sciences, 142432 Chernogolovka, Moscow District, Russia, and [d]Laboratoire des Matériaux Avancés Céramiques, Z. I. du Champ de l'Abbesse, 59600 Maubeuge, France. Correspondence e-mail: tucoulou@polycnrs-gre.fr

High-resolution X-ray diffraction measurements were carried out on ZnO/Si devices under surface acoustic wave excitation and revealed some very clear satellite diffraction peaks that are obtained from the sinusoidal modulation of the near-surface region. This experiment shows that the propagation of a Rayleigh surface acoustic wave in a perfect crystal acts as a dynamical diffraction grating. The variation of the acoustic velocity has been followed across the crystal surface from the acoustic source region (beneath the ZnO film) to the far field region (not covered by the ZnO film).

1. Introduction

X-ray diffraction has been used to study the characteristics of ultrasonic fields propagating inside crystals (see *e.g.* Cerva & Graeff, 1984; Entin, 1990; Zolotoyabko & Sander, 1995; Zarka *et al.*, 1994; Liss *et al.*, 1997; Sauer *et al.*, 1997). Ultrasonic waves have directly provided an effective tool for the modulation and the control of the spatial and temporal structure of an X-ray beam (Hauer & Burns, 1975; Kikuta *et al.*, 1984; Mkrtchyan, Navasardyan, Gabrielyan & Kocharyan, 1986; Mkrtchyan, Navasardyan, Kocharyan *et al.*, 1986). Following this approach, surface acoustic waves (SAWs) have been used in X-ray optics for generating dynamical gratings at the surface of a crystal (Roshchupkin *et al.*, 1992, 1997). The main result of the interaction of X-rays with SAWs is the rise of very strong diffraction satellites in the reflectivity measurements. Several experiments have already been carried out on Bragg diffraction on SAWs in lithium niobate crystals (Zolotoyabko & Polikarpov, 1998; Polikarpov *et al.*, 1999; Tucoulou *et al.*, 2000). Very recently, SAW-induced diffraction satellites were observed in synchrotron experiments with GaAs-based SAW devices (Sauer *et al.*, 1999).

In the case of silicon crystals, some studies of the effects of SAWs on diffraction profiles have been performed but diffraction satellites were not observed (Zolotoyabko *et al.*, 1992, 1994, 1993; Sander *et al.*, 1995). The use of the high-quality beam provided by the ESRF combined with high-resolution diffraction techniques has allowed us to observe these diffraction satellites. Here, we present experimental results demonstrating the new possibilities of X-ray diffraction for the investigation of SAW propagation on perfect silicon crystals. Taking advantage of the high penetration depth of X-rays (a few micrometres), it has been possible to study acoustic fields in deep layers under the surface and to characterize the variations of the acoustic velocity across the crystal surface.

2. Acoustics

(001) silicon substrates (20 × 10 × 1 mm) were polished with a roughness of approximately 5 Å. Since silicon is not a piezoelectric material, the standard method of exciting SAWs involves overlaying an interdigital transducer (IDT) with a thin piezoelectric film. Sputtered zinc oxide has one of the highest piezoelectric coupling constants of known films and is the most widely used for SAW devices integrated on silicon. An SAW excited in the ZnO film by the IDT is partially transmitted at the interface in order to propagate along the surface of the silicon substrate. An aluminium IDT with the following parameters was deposited on the silicon surface: acoustic aperture = 1 mm, resonance frequency = 365 MHz, period = 10 μm, number of pairs of fingers = 20.

Using reactive radio frequency (r.f.) sputtering (5:1 $Ar:O_2$) from a ZnO ceramic disk target as described by Remiens *et al.* (1994), ZnO films with a high degree of preferred orientation (*c* axis perpendicular to the surface) and thickness $h = 1.5$ μm were prepared at room temperature (Jenkins *et al.*, 1994).

As shown in Fig. 1, the ZnO film is patterned onto a small part of the silicon substrate covering the transducer *via* a lift-off technique. Thus, a large part (>1 cm) of the acoustic path along the silicon surface is free (not covered with the piezoelectric ZnO film).

The acoustic amplitude in the silicon crystal (under the ZnO film) can be varied from 0 to a few ångströms by varying the voltage applied to the IDT (0–10 V). The relationship between the acoustic amplitude and the voltage is assumed to be linear.

† Deceased, June 1999.

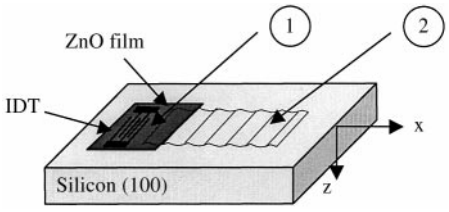

Figure 1
Scheme of the transducer overlaid by the ZnO film on the silicon crystal. The arrows 1 and 2 show the two different regions of the silicon crystal probed by the X-rays: beneath the transducer and far from it.

The propagation of an SAW in a crystal introduces, in a first approximation, a sinusoidal modulation which is superimposed on the periodicity of the crystal lattice (in fact, a Rayleigh wave is elliptically polarized, but longitudinal displacements can be omitted here). Since the phase velocity of the acoustic wave is much lower than the speed of X-rays, the acoustic deformation can be considered as quasistatic and characterized by its wavelength and amplitude.

The propagation of a Rayleigh wave at the surface of a crystal induces deformations in the bulk which extend to a depth of the order of two acoustic wavelengths, *i.e.* ~20 μm in this case. Assuming an exponential damping of the acoustic amplitude in the bulk, the variations of the acoustic wave can be written, in a first approximation, as

$$H_0 \exp(-\mu_{ac} z) \exp(i\mathbf{K}x), \quad (1)$$

where H_0 is the acoustic amplitude at the surface of the crystal, μ_{ac}^{-1} is the penetration length of the acoustic wave into the crystal depth, and $\mathbf{K}$ is the acoustic wavevector.

3. The X-ray–SAW interaction

Coherent X-ray scattering from the lateral acoustic superlattice leads to the formation of satellites on both sides of the Bragg diffraction peak. The mth order satellite appears at a specific angle α_m along which constructive interferences induced by the modulated crystal occur. In the case of Bragg geometry and transverse acoustic waves, these angular directions can be deduced from the grating equation:

$$\cos\alpha_m = m(\lambda/\Lambda) + \cos\alpha_0, \quad (2)$$

where λ is the X-ray wavelength, Λ is the acoustic wavelength, α_0 is the incident angle, m is the diffraction order and α_m is the angle of emergence of the mth order satellite with respect to the surface.

In the case of a rocking curve measurement with the detector placed in the Bragg position, $\alpha_{m\mathrm{RC}} = \theta_{\mathrm{Bragg}} + \delta\alpha_{m\mathrm{RC}}$ and $\alpha_m = 2\theta_{\mathrm{Bragg}} - \alpha_{m\mathrm{RC}}$, where $\alpha_{m\mathrm{RC}}$ is the angle of the mth order satellite given by the rocking curve. Using equation (2) and after simplification, $\delta\alpha_m$ can be written as

$$\delta\alpha_{m\mathrm{RC}} = m\lambda/2\Lambda \sin\theta_{\mathrm{Bragg}} = md/\Lambda, \quad (3)$$

where d is the interplanar spacing.

In the absence of any excitation, dynamical theory is required for the quantitative analysis of the diffraction wave field in a perfect crystal. The acoustic deformations of the crystal cause a progressive evolution of the dynamic scattering into a kinematic scattering as the acoustic amplitude increases. For the limiting cases of kinematic absorption and dynamical extinction, the X-rays penetrate roughly 21 and 2.6 μm, respectively, into the crystal, which are of the same order of magnitude as the acoustic penetration depth. This implies that most of the X-ray field interacts with the excited layer of the crystal.

4. Experimental setup

The experiment described in this paper was carried out at the optics beamline (BM05) of the ESRF. The energy (12 KeV) was selected by a double Si(111) monochromator, diffracting in the vertical plane and slightly detuned to reject harmonics.

Primary and secondary slits having horizontal and vertical gaps of 1 × 2 mm and 0.2 × 0.5 mm, respectively, were placed as shown in Fig. 2. A triple-axis diffractometer diffracting in the horizontal plane was used to obtain sufficient angular resolution (~0.1 arcsec) to separate the successive diffraction satellites clearly. Another monochromator [Si(333)] was inserted before the sample to obtain a highly monochromated beam ($\Delta\lambda/\lambda \simeq 10^{-6}$). The analyser was a single Si(333) crystal. We used a Cyberstar NaI scintillation counter for the detection.

5. Experimental results

Fig. 3 represents a two-dimensional scan around the (004) Bragg peak under SAW excitation. Very clear interference fringes are visible, proving that the dynamical grating effect occurs in the silicon crystal similar to that which was demonstrated before for a mirror (Roshchupkin *et al.*, 1992) and a multilayer structure (Roshchupkin *et al.*, 1997), and a GaAs crystal (Sauer *et al.*, 1999). Note that first-order satellites can be observed even with very small acoustic amplitudes (≤0.2 Å). For high acoustic amplitudes, they can reach 50% of the Bragg peak without SAWs. We could not measure directly the acoustic amplitude in the silicon, but it is lower than in the case of an $LiNbO_3$ crystal, which has a higher electromechanical coupling (this was confirmed by comparison of reflectivity measurements on both crystals).

Fig. 4 shows Si(004) rocking curves recorded for two nonzero acoustic amplitudes and one without acoustic excitation. It should be noted that the number of diffraction orders

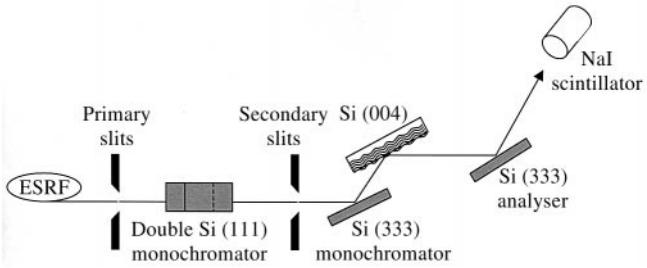

Figure 2
Experimental setup.

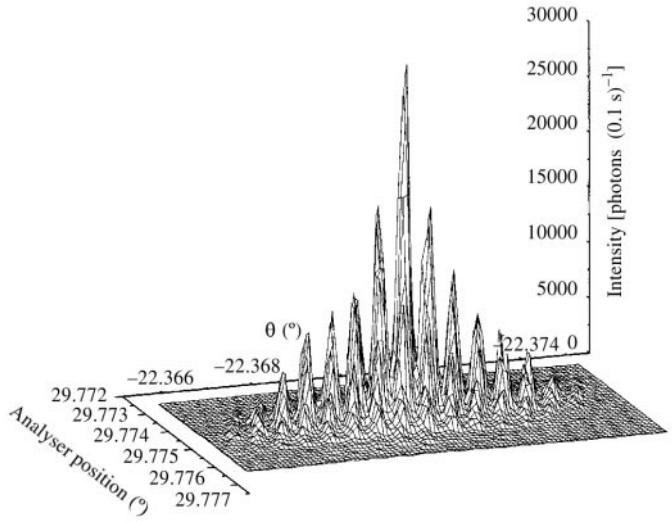

Figure 3
Map around the 004 Bragg peak showing several successive diffraction satellites.

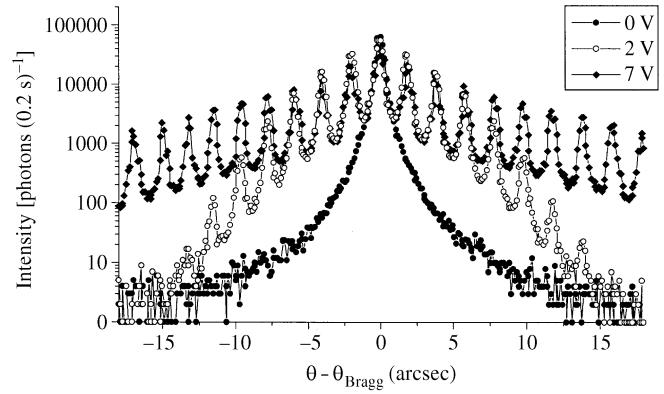

Figure 4
Rocking curves recorded for various voltages supplied to the transducer (or acoustic amplitudes).

increases with the acoustic amplitude. A specific diffraction order appears only if the acoustic amplitude reaches a threshold value. The higher the diffraction order, the higher this threshold is. Once the acoustic amplitude exceeds this threshold, the satellite intensity increases rapidly. This phenomenon is very similar to that observed in the case of diffraction on a multilayer mirror (Roshchupkin *et al.*, 1997) or on a lithium niobate crystal; it arises from the fact that the mth order satellite amplitude varies as $J_m(H_0 q_z)$ (J_m is the Bessel function and q_z is the component of the diffraction vector perpendicular to the surface) (Erko *et al.*, 1989; Tucoulou *et al.*, 2000). Each satellite has the same full width at half-maximum (FWHM) as the Bragg peak without SAWs (1.5 arcsec). These results seem to be very similar to those obtained with GaAs (Sauer *et al.*, 1999).

Fig. 5 is a plot of two rocking curves of the 004 reflection taken at two different places in the silicon crystal and with a beam width of 50 μm. In the case of the first rocking curve, the beam (number 1 in Fig. 1) hit the ZnO film and crossed it to probe the silicon crystal beneath the acoustic source. In this

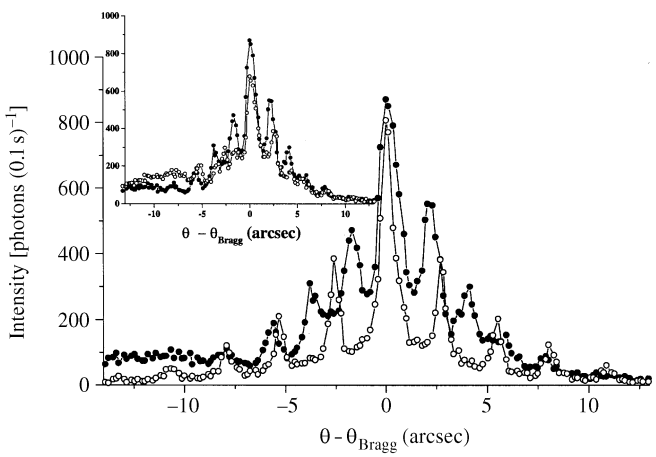

Figure 5
Rocking curves recorded at different places on the silicon crystal. Open circles: beneath the acoustic transducer. Filled circles: far from the source. The inset shows an additional rocking curve (open circles) at the boundary between the ZnO film and the free silicon.

region, the silicon crystal is forced to vibrate as the ZnO film vibrates just above it. In the second case, the X-ray beam (number 2 in Fig. 1) hit the silicon surface directly, a few mm away from the ZnO film and the transducer. In this region, the crystal vibrates freely. The voltage supplied to the transducer is 2 V in both cases. The angular positions of the adjacent diffraction satellites differ considerably. This shows that the acoustic parameters are different in the two regions. The acoustic velocity can be derived from (3) as

$$v = mdf/\delta\alpha_{m\mathrm{RC}}, \tag{4}$$

with the acoustic frequency f = 365 MHz. Equation (4) gives $v_{\mathrm{ZnO/Si}} = 3770\ \mathrm{ms}^{-1}$ and $v_{\mathrm{Si}} = 5152\ \mathrm{ms}^{-1}$. Theoretical values are $v_{\mathrm{ZnO/Si}} = 3832\ \mathrm{ms}^{-1}$ for $h/\Lambda = 0.13$ with h the thickness of the ZnO film, and $v_{\mathrm{Si}} = 5080\ \mathrm{ms}^{-1}$.

The inset in Fig. 5 shows one rocking curve taken from the free silicon region (the same as in the main graph of the figure) and the second one taken just at the boundary of the ZnO film. It can be seen on this rocking curve that most of the satellites corresponding to the free silicon have already disappeared and that new ones (corresponding to the ZnO/Si region) are growing at other positions. It is thus possible to follow precisely (within the limits of beam size) the acoustic parameter variations across the boundary between the ZnO film and the free silicon.

6. Conclusions

This experiment has shown that X-ray diffraction is very sensitive to the dynamic deformations induced by the propagation of surface acoustic waves in silicon perfect crystals. First diffraction orders can reach 50% of the Bragg peak intensity without SAWs. There is great interest in the use of silicon perfect crystals instead of $LiNbO_3$ for applications involving the time modulation of X-ray beams (Tucoulou *et al.*, 1997; Roshchupkin *et al.*, 1998).

This experiment has also shown that X-rays can probe acoustic fields in layers under the surface of a crystal. This may be of interest with regard to the characterization of integrated acousto-electronic systems consisting of a combination of semiconductors and piezoelectric materials. Simple models are under development to predict the acoustic amplitudes from the diffraction spectra.

We thank V. Zhang for the calculations of the acoustic velocities. This work has been supported by a joint program between the CNRS and the IMT in Chernogolovka. One of us (DVR) is indebted to the Russian Foundation for Basic Research (contract No. 00-02-16045). This paper is dedicated to the memory of the late Michel Brunel.

References

Cerva, H. & Graeff, W. (1984). *Phys. Status Solidi A*, **82**, 35–45.
Entin, R. (1990). *J. Appl. Cryst.* **23**, 355–358.
Erko, A. I., Roshchupkin, D. V., Snigirev, A. A., Smolovich, A. M., Nikulin, A. Y. & Vereshchagin, G. V. (1989). *Nucl. Instrum. Methods A*, **282**, 634–637.
Hauer, A. & Burns, S. J. (1975). *Appl. Phys. Lett.* **27**, 524–526.
Jenkins, D. F. L., Cunnigham, M. J., Velu, G. & Remiens, D. (1997). *Sensors Actuators A*, **63**, 135.
Kikuta, S., Takahashi, T. & Nakatani, S. (1984). *Jpn J. Appl. Phys.* **23**, L193–L194.
Liss, K. D., Magerl, A., Remhof, A. & Hock, R. (1997). *Acta Cryst.* A**53**, 181–186.
Mkrtchyan, A. R., Navasardyan, M. A., Gabrielyan, R. G. & Kocharyan, L. A. (1986). *Solid State Commun.* **59**, 147–149.
Mkrtchyan, A. R., Navasardyan, M. A., Kocharyan, L. A., Galoyan, K. G., Gabrielyan, R. G. & Unanyan, O. A. (1986). *Sov. Techn. Phys. Lett.* **12**, 629–631.
Polikarpov, I., Toledo de Oliveira, R. & Zolotoyabko, E. (1999). *Rev. Sci. Instrum.* **70**, 2230–2234.
Remiens, D., Tirlet, J. F., Jaber, B., Joire, H., Thierry, B. & Moriamez, C. (1994). *J. Eur. Ceram. Soc.* **13**, 493.
Roshchupkin, D. V., Brunel, M., de Bergevin, F. & Erko, A. I. (1992). *Nucl. Instrum. Methods B*, **72**, 471–476.
Roshchupkin, D. V., Schelokov, I. A., Tucoulou, R. & Brunel, M. (1997). *Nucl. Instrum. Methods B*, **129**, 414–418.
Roshchupkin, D. V., Tucoulou, R., Masclet, A., Brunel, M., Schelokov, I. A. & Kondakov, A. S. (1998). *Nucl. Instrum. Methods B*, **142**, 432–436.
Sander, B., Zolotoyabko, E. & Komen, Y. (1995). *J. Phys. D*, **28**, A287–A290.
Sauer, W., Metzger, T. H., Peisl, J., Avrahami, Y. & Zolotoyabko, E. (1997). *Il Nuevo Cimento*, **19D**(2–4), 455–463.
Sauer, W., Streib, M., Metzger, T. H., Haubrich, A. G. C., Wixforth, A., Peisl, J., Mazuelas, A., Härtwig, J. & Baruchel, J. (1999). *Appl. Phys. Lett.* **75**, 1709–1711.
Tucoulou, R., Mathon, O., Roshchupkin, D. V. & Schelokov, I. A. (2000). In preparation.
Tucoulou, R., Roshchupkin., D. V., Schelokov, I. A., Brunel, M., Ortega, L., Ziegler, E., Lingham, M., Mouget, C. & Douillet, S. (1997). *Nucl. Instrum. Methods B*, **132**, 207–213.
Zarka, A., Capelle, B., Pilard, M., Schwartzel, J., Detaint, J. & Solal, M. (1994). *Proceedings of the 1994 IEEE International Frequency Control Symposium*, pp. 315–322.
Zolotoyabko, E., Jacobson, E. & Shechtman, D. (1993). *J. Appl. Phys.* **73**, 8647–8649.
Zolotoyabko, E., Jacobson, E., Shechtman, D., Kantor, B. & Salzman, J. (1992). *J. Appl. Phys.* **71**, 3134–3137.
Zolotoyabko, E. & Polikarpov, I. (1998). *J. App. Cryst.* **31**, 60–66.
Zolotoyabko, E. & Sander, B. (1995). *Acta Cryst.* A**51**, 163–171.
Zolotoyabko, E., Sander, B. & Komen, Y. (1994). *Acta Cryst.* A**50**, 253–257.